

Temperature dependence of spin polarization in ferromagnetic metals using lateral spin valves

Estitxu Villamor,¹ Miren Isasa,¹ Luis E. Hueso,^{1,2} and Fèlix Casanova^{1,2*}

¹CIC nanoGUNE, 20018 Donostia-San Sebastian, Basque Country (Spain)

²IKERBASQUE, Basque Foundation for Science, 48011 Bilbao, Basque Country (Spain)

* E-mail: f.casanova@nanogune.eu

A high reproducibility in the performance of cobalt/copper and permalloy/copper lateral spin valves with transparent contacts is obtained by optimizing the interface quality and the purity of copper. This allows us to study comprehensively the spin injection properties of both ferromagnetic materials, as well as the spin transport properties of copper, which are not affected by the used ferromagnetic material, leading to long spin diffusion lengths. Spin polarizations of permalloy and cobalt are obtained as a function of temperature. Analysis of the temperature dependence of both the spin polarization and conductivity of permalloy using the standard two-channel model for ferromagnetic metals suggests that a correction factor of ~ 2 is needed for the spin polarization values obtained by lateral spin valve experiments.

I. INTRODUCTION

During the last years, lateral spin valves (LSVs) have gained an increasing attention in the field of *spintronics* [1], which aims at taking advantage of the spin degree of freedom for electronics performance. Being able to decouple the spin current from the charge current, these devices are interesting due to their potential application to information technology as well as from a fundamental point of view. LSVs consist of two ferromagnetic (FM) electrodes bridged by a non-magnetic (NM) channel (see Fig. 1(a)), which allow the electrical injection of a pure spin current from one of the FMs into the NM (and its detection with the other FM) due to their non-local geometry [2-21]. Eliminating any spurious effects coming from the charge, they provide an effective way for studying the spin transport mechanisms inside a NM material (including metals [2-9], semiconductors [10], superconductors [11] and graphene [12]), as well as the spin injection in the FM/NM system [13-21].

Despite the large number of reports employing LSVs, the dispersion in the obtained data is fairly high in literature. As an example, Table 1 shows values of the spin diffusion length of copper (Cu), λ_{Cu} , and the spin polarizations of permalloy (Py) and cobalt (Co), α_{Py} and α_{Co} , obtained from references using Py/Cu and Co/Cu LSVs with transparent interfaces. The main reason for such dispersion lies in the irreproducibility of the fabrication of the devices [4,5,21,22], due to uncontrollable factors relevant at the nanoscale, which can lead to different results. For instance, a small variation in the interface quality can induce a large change in the values of α_{Py} and α_{Co} . Regarding λ_{Cu} , it should change linearly with the inverse of the Cu channel resistivity, $1/\rho_{Cu}$ [9,23]. However, the dispersion in λ_{Cu} is too large to be solely explained by the difference in ρ_{Cu} (see Table 1). Magnetic impurities at the NM channel, which strongly decrease the spin diffusion length of a NM material, are the most likely reason for such dispersion [8,9].

In this work we show that, as a result of a careful optimization, we are able to fabricate reproducible LSVs with transparent interfaces. The values obtained from our experiments can thus be considered as a reference in LSV experiments. Such reproducibility allows a systematic analysis of Py/Cu and Co/Cu LSV systems, by studying the role both FM materials play on the spin transport in Cu and comparing their spin injection properties. Moreover, the current spin polarization of Py and Co as a function of temperature is reported for the first time for LSVs with transparent interfaces. The analysis of both α_{Py} and the conductivity of Py based on the standard two-channel model [24,25], allows us to correct a systematic underestimation of α_{Py} derived from the LSV experiments.

II. EXPERIMENTAL DETAILS

Samples were fabricated by two consecutive e-beam lithography and lift-off steps. In the first step, FM electrodes were patterned in PMMA resist on top of SiO₂(150 nm)/Si substrates and 35 nm of Py or Co were deposited in an UHV e-beam evaporator (base pressure $\leq 1 \cdot 10^{-8}$ mbar). Different widths of FM electrodes were chosen, ~ 110 and ~ 150 nm, in order to obtain different switching magnetic fields. In the second step, the NM channel with a width of ~ 170 nm and contact pads were patterned and Cu was thermally evaporated with the same base pressure $\leq 1 \cdot 10^{-8}$ mbar. Prior to the Cu deposition, in order to ensure a transparent interface, the surface of the

FM electrodes was cleaned from oxidation and resist left-overs by Ar-ion milling. This process was optimized as described below. Each sample contains up to 10 different LSVs with an edge-to-edge separation distance (L) between FM electrodes from 200 to 3500 nm. Figure 1(a) is a scanning electron microscopy (SEM) image of a device.

Non-local measurements were performed in a liquid He cryostat (with applied magnetic field H and temperatures ranging from 10 to 300 K) using a “dc reversal” technique [13]. The voltage V , normalized to the absolute value of the applied current I , is defined as the non-local resistance $R_{NL} = V / |I|$ (see Fig. 1 (a) for a scheme of the measurement). This magnitude is positive (negative) when the magnetization of the electrodes is parallel (antiparallel), depending on the value of H . The difference ΔR_{NL} between the positive and negative values of R_{NL} is called spin signal (see Fig. 1 (b)), which is proportional to the spin accumulation at the detector. Applying the one-dimensional spin-diffusion model to our geometry, the following expression is obtained for the spin signal [7,14,26]:

$$\Delta R_{NL} = \frac{2\alpha_{FM}^2 R_{NM}}{\left(2 + \frac{R_{NM}}{R_{FM}}\right)^2 e^{L/\lambda_{NM}} - \left(\frac{R_{NM}}{R_{FM}}\right)^2 e^{-L/\lambda_{NM}}}, \quad (1)$$

where α_{FM} is the spin polarization of the FM, $R_{NM} = 2\lambda_{NM}\rho_{NM}/t_{NM}w_{NM}$ and $R_{FM} = 2\lambda_{FM}\rho_{FM}/(1-\alpha_{FM}^2)w_{FM}w_{NM}$ are the spin resistances, $\lambda_{NM,FM}$ the spin diffusion lengths, $\rho_{NM,FM}$ the resistivities and $w_{NM,FM}$ the widths of the NM and the FM, respectively, and t_{NM} is the thickness of the NM. ρ_{Cu} is measured as a function of temperature for each sample, whereas ρ_{Co} ($= 11.5 \mu\Omega \text{ cm}$ at 10 K) and ρ_{Py} ($= 22.4 \mu\Omega \text{ cm}$ at 10 K) are measured separately as a function of temperature in two different devices, where the FM materials were deposited under the same nominal conditions as the FM electrodes of the LSVs. We use $\lambda_{Py} = 5 \text{ nm}$ [27] and $\lambda_{Co} = 36 \text{ nm}$ [27] at 10 K and consider a temperature dependence of the form $\lambda_{FM} = \text{const.}/\rho_{FM}$ as described in Ref. 9. Geometrical parameters are measured by SEM for each device. The values of α_{FM} and λ_{NM} are obtained by fitting ΔR_{NL} as a function of L to Eq. (1).

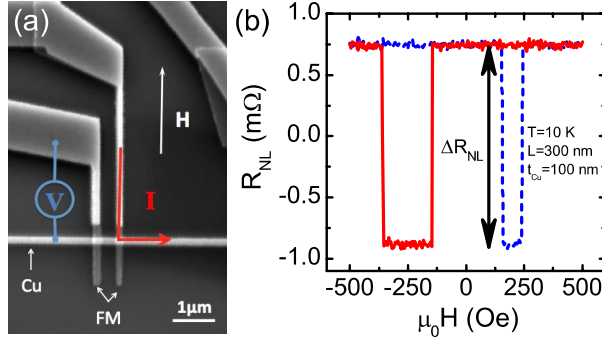


Figure 1: (a) SEM image of a typical lateral spin valve. The non-local measurement configuration, materials and the direction of the applied magnetic field H are shown. (b) Non-local resistance, measured at 10 K, for a Py/Cu lateral spin valve with $t_{Cu} = 100$ nm and $L=300$ nm. Solid red (dashed blue) line indicates the decreasing (increasing) direction of the magnetic field. Spin signal is tagged as ΔR_{NL} .

The spin injection efficiency at a transparent junction is very sensitive to the interface quality [13,17,21]. In order to optimize the interface cleaning process, α_{FM} was obtained for different samples in which the Ar-ion milling time was systematically changed. This is shown in the inset of Fig. 2 for the case of Py, where the maximum spin polarization ($\alpha_{Py} = 0.39 \pm 0.01$) is obtained for a milling time of 30 s. The other milling parameters were kept constant, with an Ar flow of 15 sccm, an acceleration voltage of 50 V, a beam current of 50 mA and a beam voltage of 300 V.

III. RESULTS AND DISCUSSION

A. Reproducibility of the lateral spin valves

As an example to show the reproducibility of our samples, Fig. 2 displays the measured ΔR_{NL} as a function of L at 10 K for 4 different Cu-based samples, 2 with Py electrodes and 2 with Co electrodes. Since the value of λ_{Cu} is influenced by the grain boundary scattering [9], the Cu channel dimensions are kept constant (with a thickness of ~ 100 nm). The results match perfectly for the 2 pairs of samples with the same FM/NM combination. In addition, since ΔR_{NL} decays nearly exponentially with L (see Eq. (1)), the slope in the semilogarithmic plot is essentially λ_{Cu} , remaining the same for all 4 samples. Furthermore, the clear shift in ΔR_{NL} for samples with different FM materials is caused by their different spin injection efficiency $\gamma = \left(\frac{2\alpha_{FM}\lambda_{FM}\rho_{FM}}{1-\alpha_{FM}^2} \right)^2$ [15], which is directly related to the intrinsic properties of the FM metal and is an important contribution to Eq. (1). The consistent results shown in Fig. 2, which have

been reproduced for virtually all samples we have fabricated (more than 20), allow us to compare properties between different samples, a long-standing problem in this type of devices [4,5,21,22].

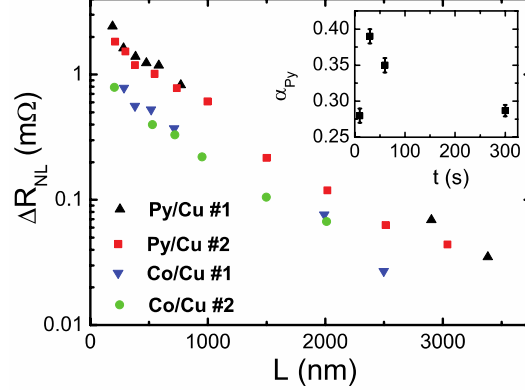


Figure 2: Spin signal as a function of the distance L between FM electrodes measured at 10 K for 4 different samples with a Cu channel and Py or Co as a FM. Inset: Spin polarization of Py as a function of the Ar-ion milling time.

B. Spin transport in Cu using different FM metals

Next, we study more in detail the role that Py and Co play in the spin transport of Cu and the spin injection properties of both FM materials. With this purpose, we obtain λ_{Cu} and α_{FM} as a function of temperature in two new samples with identical characteristics, where ~ 70 nm of Cu were deposited as the NM channel, and the FM electrodes were made of Py in one case and of Co in the other.

The values and the temperature dependence of λ_{Cu} , shown in Fig. 3, are the same for both samples containing Py and Co electrodes ($\lambda_{Cu} = 860 \pm 20$ nm and 820 ± 90 nm at 10 K for Co and Py, respectively). This is consistent with the fact that they show the same resistivity ρ_{Cu} at all temperatures ($\rho_{Cu} \sim 1.6 \mu\Omega$ cm at 10 K, see inset of Fig. 3), since λ_{Cu} is basically proportional to l/ρ_{Cu} [9]. This good agreement evidences that the use of different FM electrodes does not influence the spin transport properties of the NM channel. The obtained values of λ_{Cu} are among the highest reported in LSV experiments, given the dimensions and the ρ_{Cu} of the channel (see Table 1), further suggesting that the purity of the Cu channel is not affected by the fabrication process.

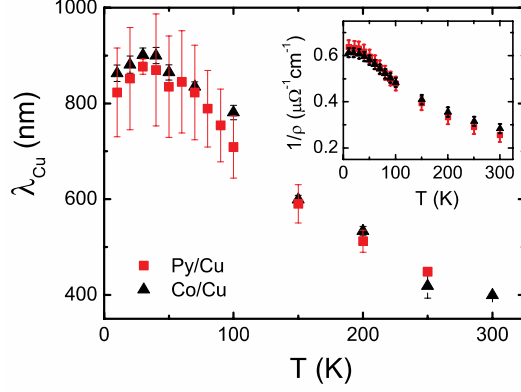


Figure 3: Spin diffusion length of Cu as a function of temperature using Py (red squares) and Co (black triangles) electrodes. A maximum is found at 30 K. Inset: Inverse of the resistivity of Cu as a function of temperature using Py (red squares) and Co (black triangles) electrodes.

Despite the saturation of $1/\rho_{Cu}$ at low temperatures, a maximum is found in λ_{Cu} for both samples, which has been previously reported for Cu- and Ag-based LSVs [5,6-9,14]. The origin of such maximum has been suggested to arise from additional spin-flip scattering at the surface of the NM channel [5-7]. This extra spin-flip scattering at the surface has been attributed to the presence of magnetic impurities [8,9], which can appear as a consequence of using a two-angle shadow evaporation process [8]. In our case, the presence of magnetic impurities at the surface of the NM channel is unlikely due to the two-step fabrication process employed. Alternatively, interdiffusion of the FM material near the interface could contaminate the NM channel. As shown in Fig. 3, the shape and position (30 K) of the maximum in λ_{Cu} is independent of the used FM material. This result confirms the previous evidence that, with our fabrication process, the NM channel is not contaminated in any way by the FM used in the electrodes. Therefore, the magnetic impurities at the bulk of the Cu channel, responsible for the maximum in λ_{Cu} , must be introduced during the evaporation process, probably from the original Cu source.

C. Spin injection properties of Py and Co

The values and temperature dependence of α_{Py} and α_{Co} are shown in Fig. 4. The values at 10 K are $\alpha_{Py} = 0.38 \pm 0.01$ and $\alpha_{Co} = 0.118 \pm 0.001$. The obtained α_{Py} is among the highest values reported in LSV experiments (see Table 1), but are usually lower (down to half) than the values obtained by other methods (0.47-0.75) [27-30]. α_{Co} is also of the same order as the highest reported values in LSV experiments with

transparent interfaces (see Table 1) and, in this case, much lower (3 to 5 times) than the values obtained by other methods (0.36-0.52) [29,31,32]. A possible explanation for the dramatic difference in Co is the uncertainty on the value of λ_{Co} , a parameter used in the fitting to Eq. (1). Co has been reported to have $\lambda_{Co} \sim 40-60$ nm [31-33], a value questioned for being much longer than those of the rest of the FM materials [23]. Since the values of α_{FM} and λ_{FM} are coupled in Eq. (1) [3] and it is not possible to obtain them independently, an overestimation of λ_{Co} would lower the fitted value of α_{Co} . The quality of the Co/Cu interface could be another reason for the low α_{Co} . Due to the natural oxidation of Co, a spin-independent interface resistance might be created between the two metals, which would act as an additional spin-flip scatterer [3]. Since this additional contribution is not taken into account in Eq. (1), it would reduce the fitted value of α_{Co} .

At this point, it should be mentioned that, even if the obtained α_{Co} is 3 times smaller than α_{Py} , the product $\alpha_{FM}\lambda_{FM}$ is twice as large for Co than for Py. The only other contribution to the spin injection efficiency γ is the electrical resistivity of the FM metal. Since ρ_{FM} is lower for Co, the backflow of the spin current is higher [15,16], making the spin injection less effective, as observed in the shift in ΔR_{NL} (Fig. 2).

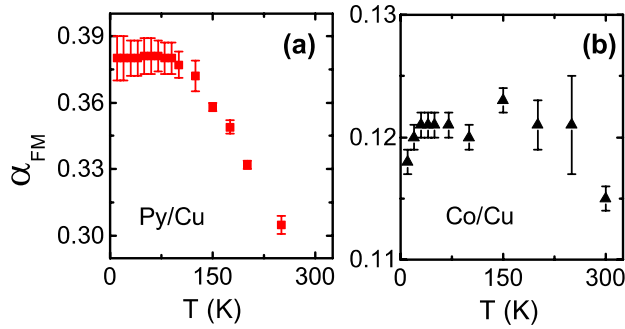


Figure 4: Spin polarization as a function of temperature for (a) Py and (b) Co. The error bars correspond to the error from the fitting of Eq. (1).

D. Temperature dependence of the spin polarization of Co and Py

In order to analyze the temperature dependence of α_{FM} extracted from the fitting of our measurements (Fig. 4), we will first note that it is an independent measurement fully decoupled from the temperature dependence of λ_{FM} , which is directly obtained from the FM resistivity [9]. It is also worth noting that the magnitude obtained from LSV experiments with transparent contacts corresponds to the current spin polarization [3]:

$$\alpha_{FM} = \frac{\sigma_{\uparrow} - \sigma_{\downarrow}}{\sigma_{\uparrow} + \sigma_{\downarrow}}, \quad (2)$$

where σ_{\uparrow} and σ_{\downarrow} are the spin-dependent conductivities introduced in Mott's two-channel model [25] and further developed by Fert and Campbell [24] in the study of electronic transport in pure ferromagnetic materials as well as in ferromagnetic alloys. However, the temperature dependence of the current spin polarization of FM metals has been only recently reported and analyzed [30,34] and, furthermore, values obtained using LSV experiments have not been studied as a function of temperature before. In the case of Co, the decay in α_{Co} is negligible up to 300 K (Fig. 4 (b)), which is expected from previous experiments [31]. In the case of Py, a clear decay in α_{Py} is observed with temperature (Fig. 4 (a)), which will allow us to analyze this dependence.

The spin-dependent conductivities can be written as:

$$\sigma_{\uparrow} = \frac{\rho_{\downarrow} + 2\rho_{\uparrow\downarrow}}{\rho_{\uparrow}\rho_{\downarrow} + \rho_{\uparrow\downarrow}(\rho_{\uparrow} + \rho_{\downarrow})} ; \sigma_{\downarrow} = \frac{\rho_{\uparrow} + 2\rho_{\uparrow\downarrow}}{\rho_{\uparrow}\rho_{\downarrow} + \rho_{\uparrow\downarrow}(\rho_{\uparrow} + \rho_{\downarrow})} \quad (3)$$

where ρ_{\uparrow} and ρ_{\downarrow} are the resistivities for spin up and down channels and $\rho_{\uparrow\downarrow}$ is the spin mixing resistance, which is a measure of the momentum transfer between the two channels by spin mixing scatterings (basically caused by electron-magnon scattering) [24,35]. The total conductivity through a FM material has thus the form:

$$\sigma_{FM} = \sigma_{\uparrow} + \sigma_{\downarrow} = \frac{\rho_{\uparrow} + \rho_{\downarrow} + 4\rho_{\uparrow\downarrow}}{\rho_{\uparrow}\rho_{\downarrow} + \rho_{\uparrow\downarrow}(\rho_{\uparrow} + \rho_{\downarrow})} \quad (4)$$

and α_{FM} can also be represented as a function of each spin-dependent resistance:

$$\alpha_{FM} = \frac{\rho_{\downarrow} - \rho_{\uparrow}}{\rho_{\uparrow} + \rho_{\downarrow} + 4\rho_{\uparrow\downarrow}}. \quad (5)$$

The temperature dependence of the three spin-dependent resistances is modeled by considering that $\rho_i = \rho_{0i} + A_i T^2$ ($i = \uparrow, \downarrow$ and $\uparrow\downarrow$), where the term ρ_{0i} accounts for spin flip-scattering due to impurities [24] and the temperature dependence comes from phonon and magnon scattering [30,34]. Hence, we can see from Eq. (5) that the increase of ρ_i with temperature will lower α_{FM} .

In order to explain the experimental temperature decay of α_{Py} with Eq. (5), coefficients ρ_{0i} and A_i will be calculated. Assuming that the spin mixing resistance, and thus $\rho_{\uparrow\downarrow}$, is zero at low temperatures [30,35], a ratio between $\rho_{0\uparrow}$ and $\rho_{0\downarrow}$ can be obtained from the low temperature values of σ_{\uparrow} and σ_{\downarrow} . The temperature dependence of σ_{\uparrow} and σ_{\downarrow} of Py is calculated from the experimental values of α_{Py} and σ_{Py} using Eq. (2) and plotted in the inset in Fig 5(a). The ratio $\rho_{0\uparrow}/\rho_{0\downarrow} = 2.2$ that we obtain is

lower than the values between 6 and 20 previously reported [24,30]. Next, A_i coefficients have been fixed as $A_{\uparrow} = A_{\downarrow} = A_{\uparrow\downarrow}$, following Ref. 36. The conductivity of Py as a function of temperature has been plotted in Fig. 5(a) and fitted to Eq. (4) (red solid line), obtaining $\rho_{0\uparrow} = (3.230 \pm 0.001) \cdot 10^{-7} \Omega \cdot \text{m}$ and $A_i = (1.96 \pm 0.01) \cdot 10^{-12} \Omega \cdot \text{m}/\text{K}^2$. According to the model above, we should be able to reproduce the temperature dependence of α_{Py} by introducing these parameters into Eq. (5). However, the obtained curve (red solid line in Fig. 5(b)) does not reproduce well the experimental temperature dependence. Alternatively, we have fitted the experimental values of α_{Py} directly to Eq. (5) (blue dashed line in Fig 5(b)) by fixing $\rho_{0\uparrow} = 3.230 \cdot 10^{-7} \Omega \cdot \text{m}$, obtaining in this case $A_i = (0.60 \pm 0.02) \cdot 10^{-12} \Omega \cdot \text{m}/\text{K}^2$. In turn, this A_i value cannot reproduce the experimental values of σ_{Py} (blue dashed line in Fig 5(a)).

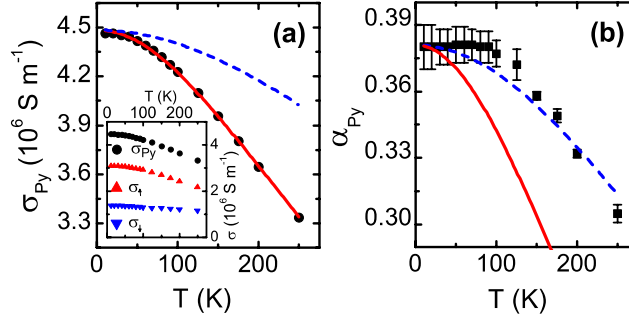


Figure 5: (a) Conductivity of Py as a function of temperature (black dots). Red solid line is a fit to Eq. (4) and blue dashed line is the representation of Eq. (4) with the $\rho_{0\uparrow}$ and A_i parameters obtained from the fitting of Eq. (5). Inset shows σ_{Py} , σ_{\uparrow} and σ_{\downarrow} as a function of temperature. (b) Spin polarization of Py as a function of temperature (black squares). Blue dashed line is a fit to Eq. (5) and red solid line is the representation of Eq. (5) with the $\rho_{0\uparrow}$ and A_i parameters obtained from the fitting of Eq. (4).

The mismatch between the red solid and blue dashed lines both in Fig. 5(a) and 5(b) evidences that the model assumed cannot simultaneously describe our two sets of independent data (α_{Py} and σ_{Py}). Considering the validity of the model to explain the temperature dependence of the current spin polarization in previous studies [30,34], it is more plausible to think that the origin of the disagreement comes from the data sets. In particular, the obtained low values of α_{Py} in LSV experiments compared to other experiments (*i.e.* GMR [27,28] or spin-wave Doppler [30]), suggest an underestimation of our α_{Py} data. A reason for such underestimation could be the one-dimensional approximation of the spin-diffusion model [26] used in LSV [7,14] to derive Eq. (1). Indeed, it has already been reported [4] that such approximation does not consider the “intermediate” region of NM metal above the

FM/NM interface, which causes spins to flip before they diffuse through the NM channel, and even to flow back to the FM electrodes, underestimating the fitted α_{FM} value. Similarly, Niimi et al. [36] have recently analyzed LSV data using a 3D finite element model based on an extension of the Valet-Fert formalism, where they observe an increase in the fitted α_{Py} from 1D to 3D.

We can correct this underestimation by introducing a multiplying factor to the experimental α_{Py} values. A factor of 1.88 is found to give the best agreement between our two data sets (α_{Py} and σ_{Py}) and the model above, as well as a much closer match between our α_{Py} value and the ones obtained by other methods [27,28,30]. The inset of Fig. 6(a) shows the temperature dependence of σ_{\uparrow} and σ_{\downarrow} for Py, calculated from the experimental values of σ_{Py} and the corrected spin polarization, $\alpha^*_{Py} = 1.88 \cdot \alpha_{Py}$, using Eq. (2). With such a correction, the ratio $\rho_{0\uparrow}/\rho_{0\downarrow}$ has a value of 6, now within the range reported in Refs. 24 and 30. The parameters obtained from the fitting of σ_{Py} to Eq. (4) (red solid curve in Fig. 6(a)) are $\rho_{0\uparrow} = (2.603 \pm 0.001) \cdot 10^{-7} \Omega \cdot m$ and $A_i = (1.09 \pm 0.01) \cdot 10^{-12} \Omega \cdot m/K^2$, which being introduced into Eq. (5), reproduce perfectly the experimental curve of α^*_{Py} (red solid curve in Fig. 6(b)). Similarly to what we have done for α_{Py} , we have fitted the values of α^*_{Py} directly to Eq. (5) (blue dashed line in Fig 5(b)) by fixing $\rho_{0\uparrow} = 2.603 \cdot 10^{-7} \Omega \cdot m$, and obtaining $A_i = (0.99 \pm 0.02) \cdot 10^{-12} \Omega \cdot m/K^2$. This value of A_i is now in excellent agreement with the previous one, and reproduces with high accuracy the experimental values of σ_{Py} (blue dashed line in Fig 6(a)).

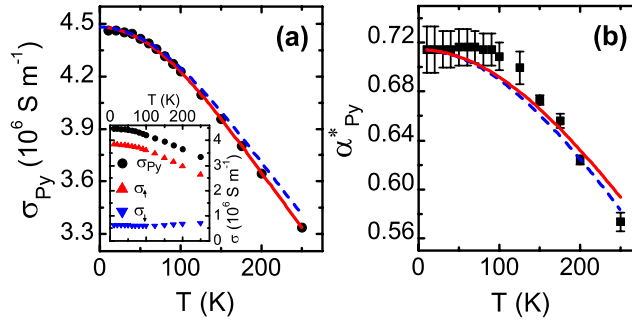


Figure 6: (a) Conductivity of Py as a function of temperature (black dots). Red solid line is a fit to Eq. (4) and blue dashed line is the representation of Eq. (4) with the $\rho_{0\uparrow}$ and A_i parameters obtained from the fitting of Eq. (5) to the corrected spin polarization of Py. Inset shows σ_{Py} , σ_{\uparrow} and σ_{\downarrow} as a function of temperature calculated with the corrected spin polarization of Py. (b) Corrected spin polarization of Py as a function of temperature (black squares). Blue dashed line is a fit to Eq. (5) and red solid line is the representation of Eq. (5) with the $\rho_{0\uparrow}$ and A_i parameters obtained from the fitting of Eq. (4).

IV. CONCLUSIONS

In summary, we succeeded in obtaining reproducible LSV devices with transparent contacts due to an optimized nanofabrication method based on a two-step lithography. This allows us to compare properties between different samples, a long-standing problem in this type of devices. Regarding the spin transport properties in Cu, the values and temperature dependence of λ_{Cu} are the same regardless of the FM material used, including a maximum at 30 K. This result shows that no contamination from the FM material into the NM channel is induced, reducing the spin-flip scattering sources and therefore enhancing the spin transport. The electrical spin injection from both Py and Co is also compared, clearly observing a decreased spin injection with the latter one, caused by its lower electrical resistivity. The experimental spin polarizations of both FM materials are among the highest reported in LSV experiments, even though they are systematically lower than those obtained by other methods. For the case of Py, based on the comparison of the temperature dependence of the spin polarization and the conductivity with the prediction given by the standard two-channel model, a correction factor of 1.88 to the spin polarization is needed. Our analysis thus confirms the substantial underestimation of the spin polarization in LSV experiments.

ACKNOWLEDGMENTS

This work is supported by the European Union 7th Framework Programme under the Marie Curie Actions (PIRG06-GA-2009-256470) and the European Research Council (Grant 257654-SPINTROS), by the Spanish Ministry of Science and Education under Project No. MAT2012-37638 and by the Basque Government under Project No. PI2011-1. E. V. and M. I. thank the Basque Government for a PhD fellowship (BFI-2010-163 and BFI-2011-106).

REFERENCES

- [1] S. Maekawa, S. O. Valenzuela, E. Saitoh, and T. Kimura, *Spin Current* (Oxford University Press, 2012).
- [2] M. Johnson and R. H. Silsbee, *Phys. Rev. Lett.* **55**, 1790 (1985).
- [3] F. J. Jedema, M. S. Nijboer, A. T. Filip, and B. J. van Wees, *Phys. Rev. B* **67**, 085319 (2003).
- [4] M. Erekhinsky, A. Sharoni, F. Casanova, and I. K. Schuller, *Appl. Phys. Lett* **96**, 022513 (2010).
- [5] G. Mihajlović, J. E. Pearson, S. D. Bader, and A. Hoffmann, *Phys. Rev. Lett.* **104**, 237202 (2010).
- [6] H. Idzuchi, Y. Fukuma, L. Wang, and Y. Otani, *Appl. Phys. Lett.* **101**, 022415 (2012).
- [7] T. Kimura, T. Sato, and Y. Otani, *Phys. Rev. Lett.* **100**, 066602 (2008).
- [8] H. Zou and Y. Ji, *Appl. Phys. Lett.* **101**, 082401 (2012).
- [9] E. Villamor, M. Isasa, L. E. Hueso and F. Casanova, *Phys. Rev. B* **87**, 094417 (2013).
- [10] Y. Aoki, M. Kameno, Y. Ando, E. Shikoh, Y. Suzuki, T. Shinjo, and M. Shiraishi, *Phys. Rev. B* **86**, 081201(R) (2012).
- [11] K. Ohnishi, T. Kimura, and Y. Otani, *Appl. Phys. Lett.* **96**, 192509 (2010).
- [12] M. H. Guimarães, A. Veligura, P. J. Zomer, T. Maassen, I. J. Vera-Marun, N. Tombros, and B. J. van Wees, *Nano Lett.* **12**, 3512 (2012).
- [13] Y. Ji, A. Hoffmann, J. E. Pearson, and S. D. Bader, *Appl. Phys. Lett.* **88**, 052509 (2006).
- [14] F. Casanova, A. Sharoni, M. Erekhinsky, and I. K. Schuller, *Phys. Rev. B* **79**, 184415 (2009).
- [15] G. Bridoux, M. V. Costache, J. Van de Vondel, I. Neumann, and S. O. Valenzuela, *Appl. Phys. Lett.* **99**, 102107 (2011).
- [16] S. Oki, S. Yamada, N. Hashimoto, M. Miyao, T. Kimura, and K. Hamaya, *Appl. Phys. Express* **5**, 063004 (2012).
- [17] T. Kimura, Y. Otani, J. Harmle, *Phys. Rev. B* **73**, 132405 (2006).
- [18] X.J. Wang, H. Zou, L. E. Ocola, R. Divan, and Y. Ji, *J. Appl. Phys.* **105**, 093907 (2009).

- [19] T. Kimura, N. Hashimoto, S. Yamada, M. Miyao, and K. Hamaya, *NPG Asia Materials* **4**, e9 (2012).
- [20] M. Erekhinsky, F. Casanova, I. K. Schuller, and A. Sharoni, *Appl. Phys. Lett* **100**, 212401 (2012).
- [21] P. Łączkwoński, L. Vila, S. Ferry, A. Marty, J. M. George, H. Jaffrés, A. Fert, T. Kimura, T. Yang, Y. Otani, and J. P. Attané, *Appl. Phys. Express* **4**, 063007 (2011).
- [22] H. Zou, X. J. Wang, and Y. Ji, *J. Vac. Sci. Technol. B* **28**, 1314 (2010).
- [23] J. Bass and W. P. Pratt, *J. Phys.: Condens. Matter* **19**, 183201 (2007).
- [24] I. A. Campbell and A. Fert, *Ferromagnetic Materials* (North-Holland, Amsterdam, 1982), Vol. 3, Chap. 9.
- [25] N. H. Mott, *Proc. Roy. Soc. A* **153**, 699 (1936).
- [26] T. Valet and A. Fert, *Phys. Rev. B* **40**, 7099 (1993).
- [27] S. Dubois, L. Piraux, J. M. George, K. Ounadjela, J. L. Duvail, and A. Fert, *Phys. Rev. B* **60**, 477 (1999).
- [28] S. D. Steenwyk, S. Y. Hsu, R. Loloee, J. Bass, and W. P. Pratt, Jr., *J. Magn. Magn. Mater.* **170**, L1 (1997).
- [29] B. Nadgorny, R. J. Soulen, M. S. Osofsky, I. I. Mazin, G. Laprade, R. J. M. van de Veerdonk, A. A. Smits, S. F. Cheng, E. F. Skelton, and S. B. Qadri, *Phys. Rev. B* **61**, R3788 (2000).
- [30] M. Zhu, C. L. Dennis, and R. D. McMichael, *Phys. Rev. B* **81**, 140407 (R) (2010).
- [31] L. Piraux, S. Dubois, A. Fert, and L. Belliard, *Eur. Phys. J. B* **4**, 413 (1998).
- [32] B. Doudin, A. Blondel, and J. P. Ansermet, *J. Appl. Phys.* **79**, 6090 (1996).
- [33] A. C. Reilly, W.-C. Chiang, W. Park, S. Y. Hsu, R. Loloee, S. Steenwyk, W. P. Pratt, Jr., and J. Bass, *IEEE Trans. Magn.* **34**, 939 (1998).
- [34] K. Ueda, T. Koyamaya, R. Hiramatsu, D. Chiba, S. Fukami, H. Tanigawa, T. Suzuki, N. Ohshima, N. Ishiwata, Y. Nakatani, K. Kobayashi, and T. Ono, *Appl. Phys. Lett.* **100**, 202407 (2012).
- [35] A. Fert, J.-L. Duvail, and T. Valet, *Phys. Rev. B* **52**, 6513 (1995).
- [36] Y. Niimi, Y. Kawanishi, D. H. Wei, C. Deranlot, H. X. Yang, M. Chshiev, T. Valet, A. Fert, and Y. Otani, *Phys. Rev. Lett.* **109**, 156602 (2012).

Table I: Resistivity and spin diffusion length of Cu and spin polarizations of Py and Co extracted from several references using Py/Cu and Co/Cu LSVs with transparent interfaces.

T (K)	ρ_{Cu} ($\mu\Omega$ cm)	λ_{Cu} (nm)	α_{Py}	α_{Co}	Reference
4.2	2.8	1000	0.2		3
10	1.36	200		0.074	13
77	1.14	1500	0.25		17
10	0.69	1000	0.58		7
4.2	1.67	395	0.29		14
4.2	--	190-260		0.1	18
4.2	--	100-400	0.15-0.4		4
4.2	1.5	460	0.21		8
80	1.2	1300	0.35		19
4.2	4	400	0.33		20
10	1.18	1020	0.4		9
10	1.6	820,860	0.38	0.12	This work